Modeling of light-induced degradation due to Cu precipitation in p-type silicon. II. Comparison of simulations and experiments

H. Vahlman,[1,a)] A. Haarahiltunen,[1] W. Kwapil,[2] J. Schön,[2] A. Inglese,[1] and H. Savin[1]
[1]*Department of Electronics and Nanoengineering, Aalto University, Tietotie 3, 02150 Espoo, Finland*
[2]*Fraunhofer Institute for Solar Energy Systems ISE, Heidenhofstr. 2, 79110 Freiburg, Germany*

(Received 30 January 2017; accepted 1 May 2017; published online 15 May 2017)

The presence of copper impurities is known to deteriorate the bulk minority carrier lifetime of silicon. In p-type silicon, the degradation occurs only under carrier injection (e.g., illumination), but the reason for this phenomenon called copper-related light-induced degradation (Cu-LID) has long remained uncertain. To clarify the physics of this problem, a mathematical model of Cu-LID was introduced in Paper I of this article. Within the model, kinetic precipitation simulations are interlinked with a Schottky junction model for electric behavior of metallic precipitates. As this approach enables simulating precipitation directly at the minority carrier lifetime level, the model is verified in this second part with a direct comparison to the corresponding degradation experiments and literature data. Convincing agreement is found with different doping and Cu concentrations as well as at increased temperature, and in the dark, both simulated degradation and measured degradation are very slow. In addition, modeled final lifetimes after illumination are very close to experimental final lifetimes, and a correlation with the final precipitate size is found. However, the model underestimates experimentally observed differences in the degradation rate at different illumination intensities. Nevertheless, the results of this work support the theory of Cu-LID as a precipitate formation process. Part of the results also imply that heterogeneous nucleation sites play a role during precipitate nucleation. The model reveals fundamental aspects of the physics of Cu-LID including how doping and heterogeneous nucleation site concentrations can considerably influence the final recombination activity. *Published by AIP Publishing.*
[http://dx.doi.org/10.1063/1.4983455]

I. INTRODUCTION

A complete mathematical model for simulating copper-related light-induced degradation (Cu-LID) at the minority carrier lifetime level was proposed in Paper I[45] of this two-part contribution. In the following, the contents of the first part are briefly summarized to provide a context for the results presented in this paper in which the model is verified with experiments. Based on earlier findings in the literature, reviewed in Paper I, it is conceivable that Cu-LID is a precipitation process of positively charged interstitial Cu (Cu_i^+) ions, forming metallic Cu_3Si precipitates that are highly recombination active in the Si bulk. Therefore, the model is based on a fundamental premise according to which the evolution of a supersaturated solid solution of interstitial Cu toward its thermal equilibrium precipitated state is retarded, in p-type Si, by electrostatic repulsion from the positively charged Cu_3Si precipitate nuclei. Growth and dissolution rates of a kinetic precipitation model, originally derived for electrically neutral spherical precipitates, were modified to include this electrostatic effect. In addition, a Schottky junction model[1–4] for metallic precipitates in Si was utilized to calculate the precipitate-related electric field. Consequently, it was shown that the magnitude of the electric field can vary considerably depending on the excess electron concentration and that precipitation kinetics can change even five orders of magnitude depending on whether the sample is illuminated or resides in the dark. This kinetic effect was interpreted to provide a possible explanation for Cu-LID. Since the mentioned Schottky model also allows the calculation of the precipitate-limited minority carrier lifetime, the full procedure for simulating lifetime degradation due to Cu precipitation with respect to illumination time was described.

Several aspects of Cu-LID have been studied experimentally in previous articles, where, for example, dependences on Cu concentration,[5] temperature,[5,6] bulk microdefect density,[7] substrate growth method,[8,9] dopant concentration,[5] and dopant type[10] have been addressed. In this article, in addition to providing new experimental data, we take another look at some of the previously published results. The fact that the proposed model works at the minority carrier lifetime level, which is one of the most accessible quantities describing the properties of a semiconductor, makes comparison to experiments particularly straightforward. Consequently, internal mechanisms of the model can be studied to understand fundamental changes imposed on the precipitation process when, for example, the above mentioned material and environmental parameters are varied. Due to the fact that a high density of small precipitates can provide a considerably larger recombination surface for minority charge carriers than a low density of large precipitates, the details of the precipitate nucleation and growth process are important from the point of view of final recombination activity of Cu-LID. Therefore, in addition to providing an estimation of the final precipitate

a)Electronic mail: henri.vahlman@aalto.fi.

size, we are able to specify factors (e.g., doping and heterogeneous nucleation site concentrations) that influence recombination losses deriving from this defect mechanism.

II. MATERIALS AND METHODS

A. Experimental details

Table I summarizes the wafer types analyzed in this work. All wafer types are boron-doped ⟨100⟩-oriented monocrystalline electronic-grade silicon. Interstitial oxygen concentrations, $[O_i]$, in Table I are given by the manufacturer for the Czochralski (Cz) wafers, and a typical (very low) value is reported for the float zone (FZ) material.

The wafers were cleaned with the standard RCA process and surface passivated by thermal oxidation at 900 °C for 40 min in O_2, followed by a 20 min anneal at 900 °C in the N_2 atmosphere. Cu contamination was performed with the spin coating method using a 1 ppm (w/v) Cu solution, followed by in-diffusion at 800 °C in an N_2 atmosphere for 20 min. The wafers were pulled out of the furnace at 800 °C and cooled in air. Temperature ramp during cooling was measured from the wafer surface with an infrared thermometer. With the 1 ppm solution, the in-diffused bulk interstitial Cu concentration, marked $C_{Cu_i}^{init}$ in the text, was estimated to be 0.76×10^{14} cm^{-3}, 1×10^{14} cm^{-3}, and 1.6×10^{14} cm^{-3} in 525 μm, 400 μm, and 250 μm thick wafers, respectively. These estimations are based on earlier work involving transient ion drift [TID, detection limit $\sim 10^{11}$ cm^{-3} (Ref. 11)] measurements,[7] and assuming that the in-diffused concentration scales directly with a wafer thickness. To prevent out-diffusion of the interstitial Cu ions and improve surface passivation provided by the thermal oxide, the wafers were double-side corona charged with a surface charge of +260 nC cm^{-2}.

The wafers were illuminated using either an LED lamp (illumination intensity corresponding to <1 sun) with a peak wavelength at 540 nm or a halogen lamp (≥1 sun) with a slightly broader spectrum peaking at 590 nm. Illumination intensity (0.003–1.8 sun) was measured using a Si photodiode-based pyranometer. The wafer surface temperature was monitored with a K-type thermocouple, verifying that the wafer surface temperature remained at approximately 25 °C under illumination. The minority carrier lifetime was measured with Sinton Instruments WCT-120 quasi-steady-state photoconductance (QSSPC) lifetime measurement equipment using a peak flash intensity of ~5 W cm^{-2} at room temperature (RT). The lifetime was measured as a function of illumination time manually (for illumination intensity ≥1 sun) or with an automated setup (<1 sun) such that at preset intervals the LED lamp turned off for the duration of the QSSPC measurement while the sample remains on the QSSPC stage throughout the measurement of the entire LID curve. This minimizes the error from the slightly varying measurement position and inaccuracy in illumination time associated with manual measurements, which involve moving the sample between the lamp and the QSSPC stage. Unless otherwise mentioned, the lifetime is reported at an excess carrier concentration $\Delta n_e = 0.1 \times N_a$, where N_a is the acceptor concentration.

TABLE I. Details of the wafer types analyzed in this work, including the growth method, resistivity, wafer thickness, and interstitial oxygen concentration $[O_i]$.

Wafer type	Growth method	Resistivity (Ω cm)	Thickness (μm)	$[O_i]$ (cm^{-3})
Low-res FZ	FZ	1.0	250	$<1 \times 10^{16}$
Low-res Cz	Cz	3.4–3.9	400	$>7 \times 10^{17}$
High-res Cz	Cz	18–22	525	$5.5–6.5 \times 10^{17}$

The generation rate in the wafers, required for the simulations, was determined from

$$G = \left(\int_0^{hc/E_G} \frac{E(\lambda)}{hc/\lambda} \times (1 - R(\lambda)) d\lambda \right) \Big/ w, \qquad (1)$$

where λ is the wavelength of light, $E(\lambda)$ is the spectral irradiance of the light source at wavelength λ, $R(\lambda)$ is the λ-dependent front reflectance of the wafer, h is the Planck constant, c is the speed of light in air, E_G is the energy gap of Si, and w is the wafer thickness. Spectral irradiance was measured with a USB spectrometer, and the front reflectance with a ultraviolet-visible-near infrared (UV-VIS-NIR) spectrometer. Due to the thickness of the wafers and the illumination spectra of the LED and the halogen light sources lacking wavelengths above 860 nm, transmittance through the wafer was considered negligible.

B. Details of calculating the effective minority carrier lifetime

The simulated effective lifetime, τ_{eff}, was calculated assuming five different recombination channels, including the Cu precipitates, fast recombination center (FRC) and slow recombination center (SRC) of the boron-oxygen (BO) defect, Auger/radiative recombination, and background/surface recombination. Instead of the full model, the precipitate-limited lifetime at RT was calculated using a parametrization based on the Schottky junction model.[4] Nevertheless, at the relevant excess carrier concentration interval of $\Delta n_e = 10^{12}$–10^{16} cm^{-3}, the full model has been found to provide results that are practically independent of the exact value of the Schottky barrier height as measured from the conduction band edge, Φ_{Bn}, in a range from 0.45 to 0.7 eV. Therefore, lifetimes determined from the parametrization do not significantly differ from the results provided by the full model in the mentioned Φ_{Bn} range.[4]

Initial injection-dependent τ_{eff}, assumed to be limited by background, surface, Auger, and radiative recombination, was taken from experimental QSSPC data separately for each sample. If this experimental information was unavailable (in the case of LID data from the literature), an injection-independent background/surface recombination-limited lifetime was assigned, which was corrected for Auger and radiative recombination with the parametrization of Richter *et al.*[12] This simplification was found to have negligible effects on simulation results at intensities exceeding 0.1 sun.

Since the Cz wafers in Table I have a high O_i concentration, they are, in addition to Cu-LID, also susceptible to LID

due to the BO defect.[13] The effect of the BO defect was calculated via the Shockley–Read–Hall (SRH) statistics using parametrized models of injection-dependent lifetime and recombination activity for both FRC[14] and SRC,[15–17] where the rate constants were taken from Schön *et al.*[18] Based on a comparison between experimental lifetime data and the lifetime given by the BO parametrization, the FRC defect concentration was found to vary between a value defined by the parametrization and a lower value, most likely due to uncontrolled degradation between sample processing and the first lifetime measurement. Therefore, to obtain good fits to experimental data, the FRC stage defect concentration was adjusted for each sample separately. However, the FRC defect considerably affects the lifetime only in the beginning of degradation, whereas its influence decreases toward the end, and the effect on the final lifetime is negligible (seen later, e.g., in Fig. 1). In the case of high-res Cz, the defect concentration of the slow SRC stage was calculated based on the parametrization of Bothe *et al.*[17] using $[O_i] = 6 \times 10^{17}\ cm^{-3}$ as given by the manufacturer. In the case of low-res Cz, however, with the minimum $[O_i] = 7 \times 10^{17}\ cm^{-3}$ given by the manufacturer the parametrization resulted in too low BO defect-limited lifetime ($\sim$75 μs at $\Delta n_e = 0.1 \times N_a$) as compared to experimental data (130–180 μs) obtained with reference wafers without Cu contamination. To improve agreement between experiments and parametrization in this case, the SRC defect concentration given by the parametrization with $[O_i] = 7 \times 10^{17}\ cm^{-3}$ was multiplied by a fixed factor of 0.43, and the obtained defect concentration value was then used in the case of all low-res Cz samples of this work (seen later e.g., Fig. 1).

In addition to Cu-LID and the BO defect, another possible source of light-induced changes in τ_{eff} comes from possible parasitic iron contamination from the Cu contamination process and consequent dissociation of Fe–B pairs to the interstitial species, Fe_i, during QSSPC measurements. Macdonald *et al.*[19] reported that a threshold flash intensity of 5 W cm^{-2} is required for Fe–B dissociation. We use this exact QSSPC flash intensity, meaning that Fe–B dissociation may occur. The influence of iron on LID curves is analyzed in Sec. III A using SRH statistics with Fe-related capture cross sections from Ref. 20.

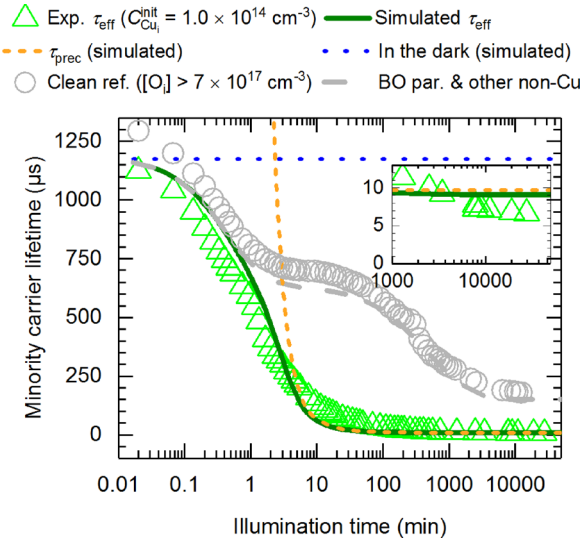

FIG. 1. Experimental Cu-LID ($[Cu] = 1 \times 10^{14}\ cm^{-3}$) and BO-LID (clean reference) under 0.65 sun intensity at RT compared to simulated τ_{eff}, τ_{prec}, and BO defect-limited minority carrier lifetime according to the modified parametrization (with $[O_i] = 7 \times 10^{17}\ cm^{-3}$, see Sec. II B) corrected for other mechanisms including background, surface, Auger, and radiative recombination. The blue dotted curve shows how the simulated lifetime remains high in the dark. Lifetimes are reported at an excess carrier concentration $\Delta n_e = 0.1 \times N_a$. The inset is a zoom from 1000 min to the end of the time scale.

III. COMPARISON BETWEEN MODEL AND EXPERIMENTS

A. Minority carrier lifetime evolution under illumination and in the dark

In Fig. 1, experimental LID data are compared with simulations and divided into components due to Cu precipitation and BO-LID. Here, we first discuss only the experimental result, and the simulations are treated separately below. Triangles show the experimental minority carrier lifetime evolution of a low-res Cz wafer with an in-diffused interstitial Cu concentration of $C_{Cu_i}^{init} = 1 \times 10^{14}\ cm^{-3}$, illuminated under 0.65 sun at RT. The experimental curve shows several distinct phases of LID, the first one taking place on a timescale of few minutes. The first phase can be closely associated with the FRC stage of the BO defect, as can be seen by comparing with the non-contaminated (clean) reference wafer in Fig. 1 (gray circles) and the lifetime given by the BO parametrization modified as described in Sec. II B (gray dashed line), corrected for the background, surface, Auger, and radiative recombination. The second degradation phase in the experimental curve causes a steep decline after a few minutes of illumination. Based on the BO parametrization, this phase cannot be explained with the BO defect and must therefore be caused by Cu. In addition, the samples of this work exhibit an asymptotic degradation phase with very slow degradation even after thousands of minutes of illumination, which was earlier observed in Ref. 5.

The experimental initial τ_{eff} of the Cu contaminated wafer in Fig. 1 is high and equal in magnitude to that in the clean reference wafers of this and earlier work,[5] which implies that at in the beginning the lifetime is not limited by Cu precipitates. In addition, it has earlier been confirmed with TID measurements that the slower cooling ramp of air cooling (on average $\sim$4 K/s from 800 °C to 100 °C as measured in this work) compared to fast quenching (comparable to a typical 60–100 K/s after solar cell metallization firing in the industry[21]) does not influence the interstitial Cu concentration after in-diffusion.[7] This implies that a negligible fraction of Cu precipitates during cooldown in both cases. This result is further supported by another study in which complete out-diffusion of Cu was observed after a pull-out from 800 °C and removal of surface oxide with similar Cu contamination levels as used in current work.[22] Therefore, since also the dark storage time of the wafers was kept brief (on the order of days) in comparison to several months it takes for any visible degradation to occur,[7,23] the simulations of this work were performed assuming that the initial interstitial Cu concentration, $C_{Cu_i}^{init}$, is the same as the in-diffused concentration, and no significant precipitation has occurred prior to illumination.

The possibility that Fe could influence the LID behavior was tested with a Cu-contaminated ($C_{Cu_i}^{init} = 0.8 \times 10^{14}$ cm^{-3}) and partially degraded low-res FZ sample ($N_a = 1.6 \times 10^{16}$ cm^{-3}) by subjecting it to repeated flashes from the QSSPC setup after first keeping it in the dark for several days. A τ_{eff} increase from 317 μs (at $\Delta n_e = 0.1 \times N_a$.) after the first flash to a saturated value of ~348 μs after 20 flashes was observed, which did not increase further despite 150 flashes being recorded in total. According to SRH statistics, this increase in τ_{eff} corresponds to [Fe] of $\sim 2 \times 10^{10}$ cm^{-3} assuming that all Fe–B pairs dissociate. Since measuring a single point in the LID curve involves two flashes, it is likely that in the beginning of the LID curve with short measurement intervals the majority of Fe exists as Fe_i, whereas at the end when the intervals are longer (≥120 min) Fe–B pairs dominate since the majority of Fe_i is expected to re-associate.[24] Nevertheless, the effect of Fe is small at low τ_{eff} when Cu precipitates are the main limiting defects (maximum increase of τ_{eff} upon full Fe–B dissociation to Fe_i diminishes to ~0.7 μs at $\tau_{eff} = 50$ μs). In lower doped low-res Cz in Fig. 1 ($N_a = 3.8 \times 10^{15}$ cm^{-3}), the maximum increase with similar [Fe] is even smaller, ~0.4 μs at $\tau_{eff} = 50$ μs and ~0.01 μs at $\tau_{eff} = 10$ μs (at $\Delta n_e = 0.1 \times N_a$). Since Fe does not notably affect analysis of Cu precipitation, dissociation and re-association kinetics of Fe-related defects was not considered in simulated LID curves of this work.

The results of simulations are reported in Fig. 1 as a solid line representing the effective lifetime, τ_{eff} (simultaneously due to Cu precipitates, the BO defect, and background, surface, Auger, and radiative recombination). The simulated τ_{eff} has been reproduced by setting the energetic terms of Eq. (2) in Paper I to $\Delta G_S = 0$ and $\gamma = 0.615 \times 10^{-4}$ J cm^{-2}, corresponding to the free energy change per precipitate volume due to strain and the interface energy, respectively, and the kinetics-related chemical activation barrier of Eq. (14) in Paper I to $\Delta G_{act} = 0$ (note that these values will be used throughout this study, and a physical interpretation will be given later in the text). Hence, the precipitate-limited lifetime, τ_{prec}, given by the Schottky model and shown in Fig. 1 as a yellow dashed line, starts limiting τ_{eff} at a similar illumination time (~2 min) as in the experimental data. The simulated τ_{eff} shows two separate degradation stages that are similar to the first two phases in the experimental data, and the final lifetimes are close to each other (i.e., 9.1 μs according to the simulation and 6.7 μs experimentally). However, the model does not reproduce the asymptotic degradation phase extending beyond thousands of minutes that was visible in the experimental data.

An important aspect to confirm with the fitted values of ΔG_S, γ, and ΔG_{act} is that precipitation in the dark should be very slow, as previously experimentally shown for Cu concentrations notably lower than N_a such as used in this work.[7,11,23,25,26] The blue dotted curve in Fig. 1 shows simulated τ_{eff} (BO defect omitted) of a low-res Cz wafer as a function of time when $\Psi_n^S = 0.31$ V, corresponding to the thermal equilibrium built-in voltage when Φ_{Bn} is set to 0.59 eV (a value associated with the Si–Cu_3Si interface[27]). In this case, the model predicts very slow precipitation, and τ_{eff} remains at the value limited by the background, surface, Auger-, and radiative recombination for ~3 weeks (500 h). However, the simulated degradation is faster than experimentally, where Cu contaminated wafers have been observed to preserve degradation-free over several months.[7,23] Therefore, it is possible that the model somewhat overestimates the degradation rate in thermal equilibrium conditions. Nonetheless, in the dark at RT, after 3 months the simulated lifetime is still ~360 μs, and full degradation does not occur until ~2.5 years. In this context, it was also verified that few days of simulated darkness before modeling the LID behavior under illumination does not influence the results in any visible way.

B. Cu concentration dependence

The response of the model on a change in Cu concentration was tested with published data from Lindroos and Savin,[5] obtained with similar wafers which also underwent the same processing steps as the low-res Cz material in Table I. Figure 2 shows experimental LID curves with two different C_{Cu}^{init} of 0.5×10^{14} cm^{-3} and 1×10^{14} cm^{-3}, both illuminated under 1 sun. Note that Fig. 2 is divided into two subfigures, where the only difference is that in (a) the minority carrier lifetime scale is linear, whereas in (b) the scale is logarithmic. The sample with the higher Cu concentration degraded faster and saturated to a lower lifetime than the sample with the lower Cu concentration, that is, 7.6 μs and 21 μs, respectively. Simulation results are shown as lines on top of the experimental LID data, and the BO defect-limited lifetime according to the parametrization (where the FRC defect concentration was adjusted to fit the $C_{Cu}^{init} = 0.5 \times 10^{14}$ cm^{-3} data) is shown for comparison as a dashed gray line. During the simulations, the energetic and kinetic terms were kept fixed at the same values as above ($\Delta G_S = 0$, $\gamma = 0.615 \times 10^{-4}$ J cm^{-2}, and $\Delta G_{act} = 0$). The LID behavior is approximately reproduced with simulated final τ_{eff} of 9.3 μs and 29 μs in the case of the higher and the lower Cu concentration, respectively. Comparing the linear scale of Fig. 2(a) to the logarithmic scale of Fig. 2(b), the latter reveals more clearly that the slope of the effective lifetime is overestimated by the model in comparison to experiments, which derives from excessively steep descent of τ_{prec}. Therefore, the model deviates from experiments in either the lower (10–100 μs) or the higher (>100 μs) lifetime range. A possible reason for this deviation will be discussed in Sec. IV E. Nevertheless, despite less than perfect agreement between simulations and experiments, the degradation rates and final degraded lifetimes between different samples are in qualitative correlation.

C. Intensity dependence

As discussed in Paper I of this article, injection conditions can considerably influence the precipitation kinetics. It is therefore relevant to investigate how well the modeled lifetime evolution agrees with experimental data at different illumination intensities. A comparison of experimental and simulated LID at intensities from 0.003 to 1.8 sun is presented in Fig. 3, where the samples correspond to low-res Cz wafers with $C_{Cu_i}^{init} = 10^{14}$ cm^{-3}. Note that the difference in initial lifetime between 0.003 sun and 0.11 sun data derives from a difference in the initially recombination active FRC

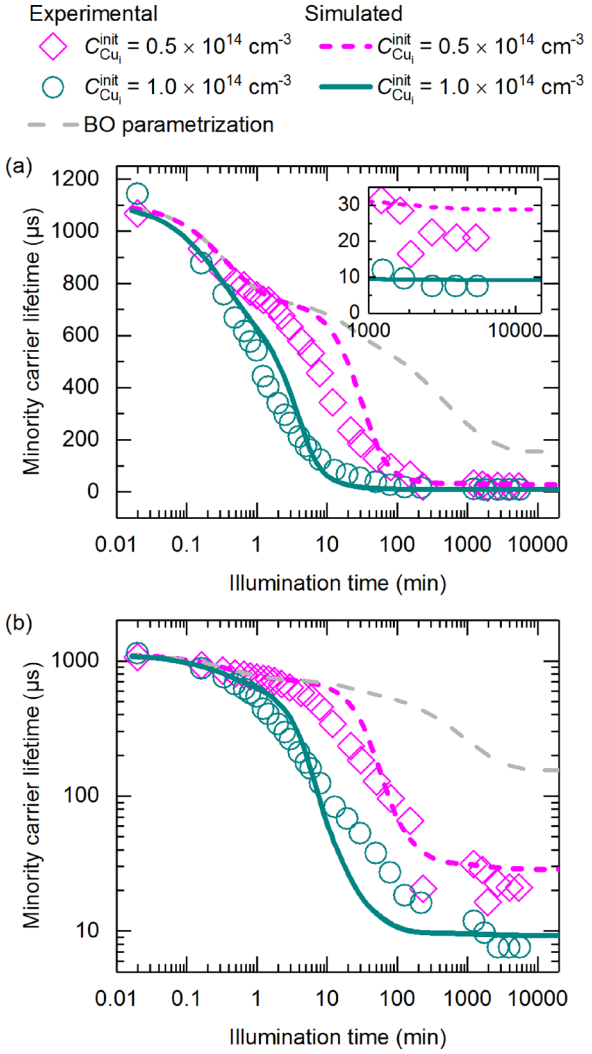

FIG. 2. Comparison of simulated LID curves with experimental data at two different Cu concentrations illuminated under 1 sun. Experimental data are from Ref. 5, and BO-limited lifetime was calculated with the modified parametrization assuming $[O_i] = 7 \times 10^{17}$ cm^{-3} (see Sec. II B). The same graph is shown with both linear (a) and logarithmic (b) minority carrier lifetime-scales. Lifetimes are reported at an excess carrier concentration $\Delta n_e = 0.1 \times N_a$. The inset in (a) is a zoom from 1000 min to the end of the time scale.

defect concentration, whereas the low initial lifetime of the 1.8 sun data may be related to a poorer surface oxide quality since this sample was processed in a separate batch in which low initial lifetimes were measured also in other samples. It was verified with the BO parametrization used in this work that the considerable intensity dependence of the experimental data differs from the limited intensity dependence of BO-LID[28] and therefore derives from Cu-LID. At the lowest intensity of 0.003 sun, the degradation continued even after 65 000 min (45 days). To speed up the degradation in this case, intensity was increased to 0.65 sun at a point marked with the asterisk (*) symbol, after which the lifetime degraded to a similar value (6.7 μs) as with higher intensities.

The intensity dependence of Cu-LID was modeled using the same energetic and kinetic terms as above ($\Delta G_S = 0$, $\gamma = 0.615 \times 10^{-4}$ J cm^{-2}, and $\Delta G_{act} = 0$) and the generation rate G was redetermined for each intensity using Eq. (1). The results, shown in Fig. 3 as lines on top of the experimental

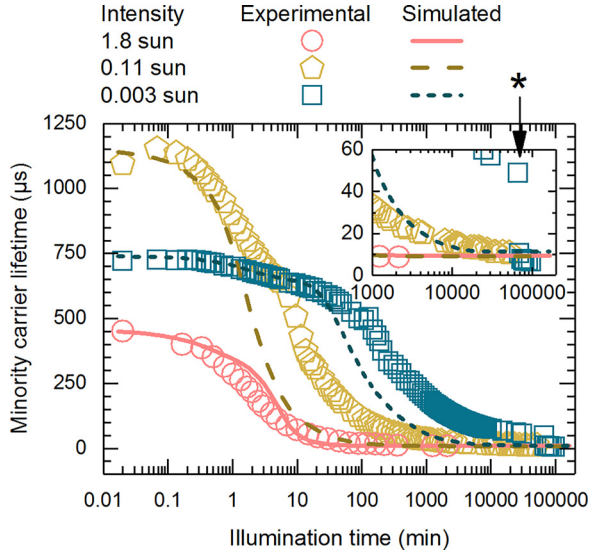

FIG. 3. Intensity dependence of Cu-LID according to experiments and simulations, taking also the BO-LID into account. Lifetimes are reported at an excess carrier concentration $\Delta n_e = 0.1 \times N_a$. The inset is a zoom from 1000 min to the end of the time scale. In the case of the 0.003 sun data, the intensity was increased to 0.65 sun after the point marked with an asterisk (*).

data, show that while the highest intensity is reproduced by the model relatively well, at lower intensities the rate of degradation is clearly overestimated. This discrepancy will be further discussed in Sec. IV C.

D. Temperature dependence: Accelerated LID

Temperature dependence of the model was tested with published data from Inglese *et al.*[6] In the mentioned study, similar samples as used in this work (low-res Cz wafers with $C_{Cu_i}^{init} = 10^{14}$ cm^{-3}) were degraded at an elevated temperature of 120 °C and found to exhibit so called accelerated LID (ALID) behavior, that is, a considerable increase in the degradation rate of Cu-LID was observed in comparison to Cu-LID at RT (RT-LID). A comparison of Cu-related ALID and RT-LID under 0.5 sun illumination is presented in Fig. 4. Experimentally, the degradation rate is considerably higher in ALID conditions, while the final lifetime remains in a similar order of magnitude as in the case of RT-LID. The degradation behavior cannot be explained by the BO defect in either case, as can be seen by comparing the experimental data with the brown and gray dashed lines in Fig. 4, which show the BO- and background/surface-limited lifetime in conditions corresponding to ALID and RT-LID, respectively. Simulated τ_{eff} curves are shown as lines on top of the experimental data (with the same values of the energetic and kinetic terms as above). It is noteworthy that, in comparison to experiments, the rate of degradation is overestimated by the simulations in both cases. This overestimation of the degradation rate most likely derives from the fact that, as discussed above in Sec. III C, the model seems to overestimate the degradation rate when the intensity is lowered (from 0.65 sun in Fig. 1 to 0.5 sun in this case). However, the main experimental characteristics of Cu-related ALID, namely, the increased rate of degradation and the similar final

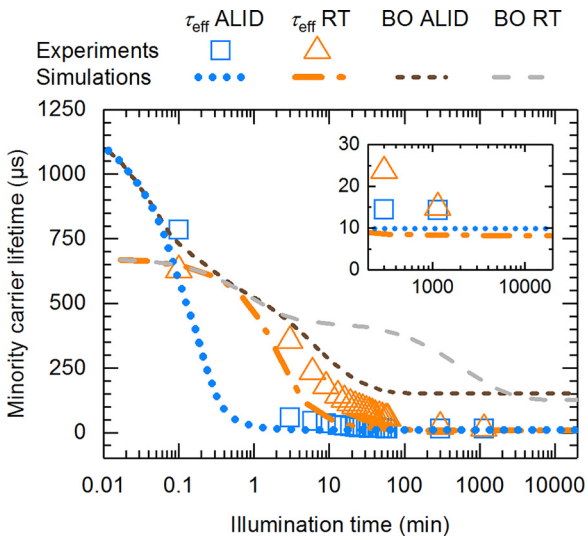

FIG. 4. Cu-related accelerated LID as predicted by the model and compared to experimental data from Ref. 6. The illumination intensity was 0.5 sun, and both samples were low-res Cz wafers with $C_{Cu_i}^{init} = 10^{14}$ cm^{-3}. Consistent with Ref. 6, the lifetimes are reported at an excess carrier concentration of $\Delta n_e = 3 \times 10^{14}$ cm^{-3}. The inset is a zoom from 200 min to the end of the time scale.

lifetime as in the case of RT-LID, are clearly visible in the simulated curves of Fig. 4.

E. Doping dependence

To investigate the effect of doping, samples with different resistivities were studied. First, Fig. 5 shows the LID curve of a low-res FZ wafer ($N_a = 1.5 \times 10^{16}$ cm^{-3}) with $C_{Cu_i}^{init} = 1.6 \times 10^{14}$ cm^{-3} under 0.65 sun, together with the LID curve of a low-res Cz wafer ($N_a = 3.8 \times 10^{15}$ cm^{-3}) with $C_{Cu_i}^{init} = 1 \times 10^{14}$ cm^{-3}, also under 0.65 sun, and earlier shown in Fig. 1. In the case of the low-res FZ sample, the FRC stage of the BO defect is absent due to an O_i concentration typically two orders of magnitude lower than in Cz wafers. Although illumination-induced minority carrier lifetime instabilities not related to the BO defect have been earlier reported in the FZ material,[29,30] our non-contaminated

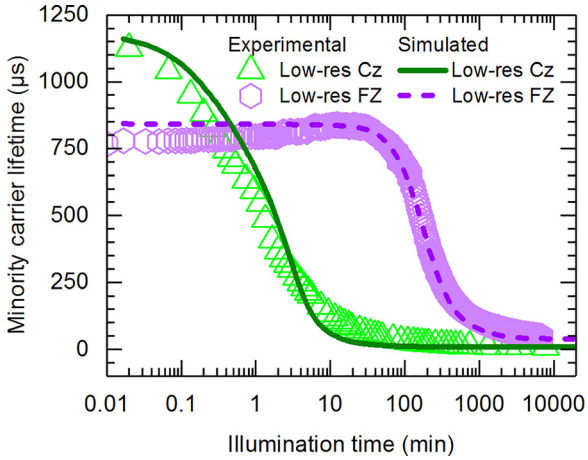

FIG. 5. Experimental and modeled Cu-LID in low-res FZ and low-res Cz samples illuminated under 0.65 sun at RT. Lifetimes are reported at an excess carrier concentration $\Delta n_e = 0.1 \times N_a$.

reference samples (not shown) showed no degradation under 0.65 sun illumination at RT for 10^4 min. It is therefore clear that, similarly to Ref. 31, the observed LID of the FZ sample in Fig. 5 arises solely from Cu-LID. On the other hand, as it was shown in Fig. 1 that the effective lifetime of the low-res Cz sample becomes heavily limited by Cu-LID after only few minutes of illumination, it can be concluded that Cu-LID is considerably slower in the low-res FZ than in the low-res Cz sample even despite the higher $C_{Cu_i}^{init}$ in the former. Simulated τ_{eff} (with the same energetic and kinetic terms $\Delta G_S = 0$, $\gamma = 0.615 \times 10^{-4}$ J cm^{-2}, and $\Delta G_{act} = 0$ as above), shown as lines, are in agreement with the experiments with coinciding degradation rates and final lifetimes. The final lifetime was 48 μs experimentally and 40 μs according to the simulation in the case of low-res FZ, which are notably higher than the respective values of 6.7 μs and 9.1 μs in the case of low-res Cz. Therefore, the experimentally observed difference between degradation rates and final lifetimes can be fully explained by the effect of differing doping concentrations on Cu-LID. The reason why doping can influence the results so heavily will be further discussed in Sec. IV.

In order to widen the doping range studied in this work, experimental data of a high-res Cz wafer ($N_a = 6.0 \times 10^{14}$ cm^{-3}) with $C_{Cu_i}^{init} = 0.76 \times 10^{14}$ cm^{-3} from Ref. 5, illuminated under 1 sun, are shown in Fig. 6 with red pentagons. Comparison with the BO defect-limited lifetime for the high-res Cz sample (gray dashed line) confirms that degradation of this sample derives from Cu-LID rather than BO-LID. Also shown for comparison are the experimental and modeled τ_{eff} of the 1 sun-illuminated low-res Cz wafer with $C_{Cu_i}^{init} = 1 \times 10^{14}$ cm^{-3}, reported in Fig. 2. In Fig. 5, a fourfold increase in N_a

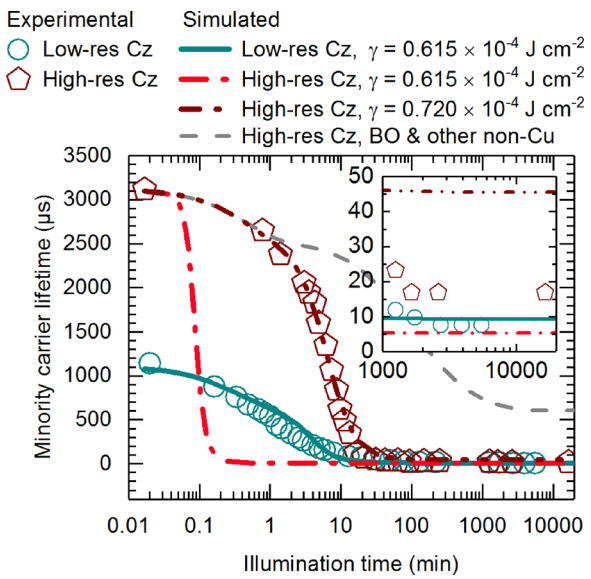

FIG. 6. Experimental and modeled Cu-LID in high-res Cz and low-res Cz samples with $C_{Cu_i}^{init}$ of 0.76×10^{14} cm^{-3} and 1×10^{14} cm^{-3}, respectively, under 1 sun at RT. High-res Cz samples were simulated separately with two values of γ, 0.615×10^{-4} J cm^{-2} and 0.720×10^{-4} J cm^{-2}. Also shown is the BO defect-limited lifetime for the low-res Cz sample under 1 sun at RT. Experimental data are from Refs. 5 and 32, and the lifetimes are reported at an excess carrier concentration $\Delta n_e = 0.1 \times N_a$. The inset is a zoom from 1000 min to the end of the time scale.

from 3.8×10^{15} cm^{-3} (low-res Cz) to 1.5×10^{16} cm^{-3} (low-res FZ) caused an approximately two orders of magnitude decrease in the degradation rate. In the high-res Cz case in Fig. 6, the decrease in N_a compared to low-res Cz is even greater (six-fold), and based on the modeling result (with the same energetic and kinetic terms $\Delta G_S = 0$, $\gamma = 0.615 \times 10^{-4}$ J cm^{-2}, and $\Delta G_{act} = 0$ as above), shown as a red dashed–dotted line, an increase of the degradation rate of almost two orders of magnitude is expected. Instead, the high-res Cz sample shows slower degradation than the low-res Cz sample, and the experimental final lifetime of 17 μs is notably higher than 7.6 μs of the low-res Cz wafer, or 5.4 μs obtained for high-res Cz with modeling.

To improve the agreement between simulated τ_{eff} and experiments, the value of the surface energy term, γ, was increased from 0.615×10^{-4} J cm^{-2} to 0.720×10^{-4} J cm^{-2} as shown by the dashed–double dotted line in Fig. 6. With this higher value of γ, not only does the degradation rate decrease to coincide with the experimental high-res Cz data but also the final lifetime increases from 5.4 μs to 45 μs, qualitatively reproducing the experimentally observed reduction in the degradation rate and increase in the final lifetime in comparison to low-res Cz. A physical interpretation for this adjustment of γ is provided in Sec. IV.

F. Injection dependence

While Secs. III A–III E focused on minority carrier lifetime at a single excess carrier concentration ($\Delta n_e = 0.1 \times N_a$) as a function of illumination time, here simulation results are compared to experimental final degraded lifetimes measured over a broad range of excess carrier concentrations. The samples included in this analysis are the low-res Cz wafer in Fig. 1 (degraded at RT), the low-res Cz wafer in Fig. 4 (degraded under ALID conditions), and the low-res FZ wafer in Fig. 5. Since the measured lifetime is affected by many recombination processes (e.g., radiative, Auger, surface, and BO defect recombination), the Cu-related lifetime, τ_{Cu}, has been separated from the other recombination channels through the relation

$$\tau_{Cu}(\Delta n_e) = \left(\frac{1}{\tau_{deg}} - \frac{1}{\tau_{init}} - \frac{1}{\tau_{BO}} \right)^{-1}, \quad (2)$$

where τ_{deg} and τ_{init} are the injection-dependent lifetimes measured before and after degradation, and τ_{BO} is the BO-related lifetime in the final degraded state, calculated with the BO parametrization used in this work. Here, we note that Fe is expected to be approximately in the same state (mostly existing as Fe–B, see Sec. III A) both before and after degradation, and its (small) effect is therefore accounted for by Eq. (2). Figure 7 reports τ_{Cu} and simulated injection-dependent lifetime curves that were calculated using the final precipitate size and density distributions resulting from the simulation of the LID curves (discussed further in Sec. IV D) and the parametrization of Ref. 4. Good agreement between simulated and experimental lifetime curves can be observed in all cases. Importantly, the overall shape of the modeled curves is in substantial agreement with the experimental data.

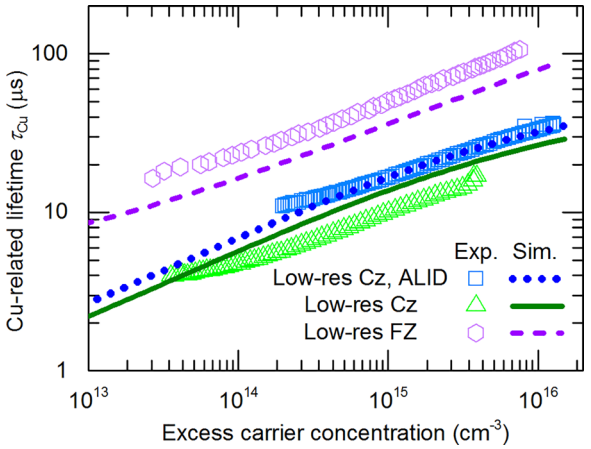

FIG. 7. Experimental and simulated injection-dependent minority carrier lifetimes in the final degraded state in the case of low-res Cz and FZ samples of Figs. 1, 4, and 5. The experimental lifetime data were corrected for other mechanisms unrelated to Cu-LID, including radiative, Auger, surface, and BO defect recombination.

IV. ANALYSIS AND DISCUSSION

In Secs. IV A–IV E, the internal mechanisms of the model are investigated further. Considering the good qualitative agreement that was found between simulations and experiments in Sec. III, we believe that this analysis can be extended to real-life samples and can help improve the general understanding of the physical phenomena that take place during Cu-LID. To summarize, the correlation between the energetic barrier of nucleation and precipitate density is illustrated in Sec. IV A. In addition, the connection between the degradation rate of Cu-LID and nucleation rate (NR) is examined in Sec. IV B, followed by a discussion on the kinetics of Cu-LID in Sec. IV C. Furthermore, a clear link is drawn between the final lifetime and precipitate size in Sec. IV D. Finally, in Sec. IV E, the physical significance of the above fitted energetic parameters, γ and ΔG_S, is discussed together with considerations regarding the nucleation mode of Cu-LID.

A. Precipitate density

Precipitate density is considerably dependent on the energetics of the nucleation process. While growth of existing nuclei larger than critical size occurs spontaneously, the nucleation stage demands external energy.[33] In case the interstitial Cu ions do not have sufficient energy for nucleation to continue, the precipitation process continues only with the growth of existing nuclei, and the precipitate density remains constant. Energetics of nucleation can be examined by solving the effective nucleation barrier (NB) height, corresponding to the total energy required to grow a precipitate from an interstitial atom to the critical size (including electrostatic effects), based on Eq. (1) in Paper I using the above fitted values of γ and ΔG_S.

In Fig. 8, the effective NB height at the start of illumination, when the interstitial Cu concentration is still at its initial value, is correlated with final precipitate density obtained from the simulations in the different cases described in Figs. 2, 4, 5, and 6. The initial NB height reduces in the order of

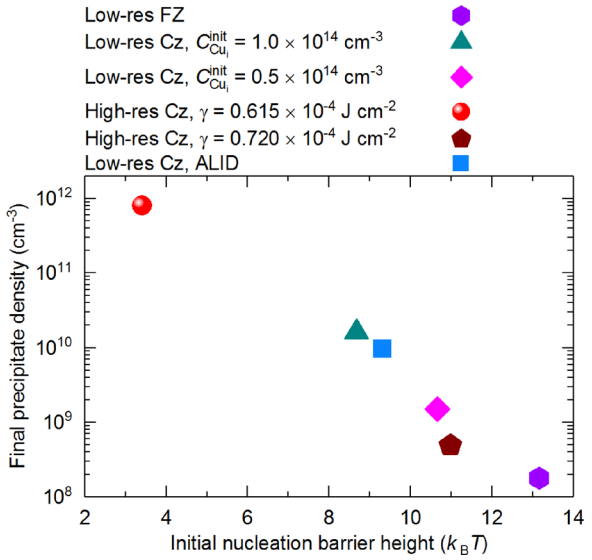

FIG. 8. Final precipitate density after illumination obtained from the simulations as a function of the initial NB height.

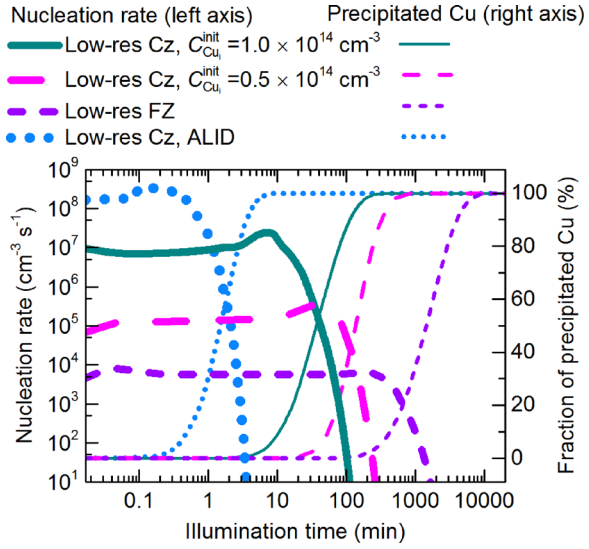

FIG. 9. Simulated nucleation rate (left axis) and precipitated Cu fraction (right axis) as a function of illumination time in the different cases described by Figs. 2, 4, and 5.

decreasing doping due to declining solid solubility, which can be associated with a clear trend of increasing precipitate density. On the other hand, halving the interstitial Cu concentration from 1×10^{14} cm^{-3} to 0.5×10^{14} cm^{-3} (low-res Cz) increases the NB height from $8.7 \times k_B T$ to $11 \times k_B T$, which also illustrates how the energetics changes as interstitial Cu ions are consumed as precipitation progresses. Moreover, the rise in NB height when γ is increased from 0.615×10^{-4} J cm^{-2} to 0.720×10^{-4} J cm^{-2} in the high-res Cz case not only reduces the degradation rate of Cu-LID in Fig. 6 but also considerably decreases the precipitate density (increasing final τ_{eff}).

B. Nucleation rate

The degradation rate of Cu-LID can be closely correlated with the initial rate of nucleation. To illustrate this dependence, Fig. 9 shows the nucleation rate (NR) for different experimental cases in Figs. 2, 4, and 5, describing how many stable nuclei (above critical size) are formed under illumination per unit volume and time.

In the case of the low-res Cz sample with $C_{Cu_i}^{init} = 1 \times 10^{14}$ cm^{-3}, the initial NR starts from a stable value of $\sim 10^7$ cm^{-3} s^{-1}. After ~20 min of illumination, there is a steep descent in NR, which can be associated with a decrease in the level of supersaturation due to consumption of interstitial Cu (or increased fraction of precipitated Cu shown on the right axis of Fig. 9). The effect of decreased interstitial Cu concentration is further illustrated by the low-res Cz sample case with $C_{Cu_i}^{init} = 0.5 \times 10^{14}$ cm^{-3}, in which the initial NR is two orders of magnitude lower than with $C_{Cu_i}^{init} = 1 \times 10^{14}$ cm^{-3}, only $\sim 10^5$ cm^{-3} s^{-1}, which explains the lower degradation rate of this sample in Fig. 2.

Also shown in Fig. 9 is the nucleation rate in low-res FZ, whose low value explains the slow degradation in Fig. 5. The difference between the NRs of low-res Cz and low-res FZ derives mostly from the greater NB height in the latter (see Fig. 8), and in a smaller part from the ~3.5 times lower diffusivity in the low-res FZ material, which is due to the higher N_a and Cu–B pairing. In the case of ALID, on the other hand, the initial NB height in Fig. 8 is $9.3 \times k_B T$, that is, only slightly higher than $8.7 \times k_B T$ of the similar low-res Cz wafer at RT. This means that energetics cannot explain the greatly increased nucleation rate of ALID (blue dotted curve in Fig. 9), but kinetics, that is, precipitate surface effects limiting the growth process, must be considered.

C. Kinetics of Cu-LID

Kinetics is affected first by the interface reaction rate [see Eq. (14) in Paper I] and second by depletion of interstitial Cu at the precipitate surface in comparison to the general bulk concentration in the sample. Considering that the best agreement between experiments and simulations was obtained by assuming a negligible activation barrier of the interface reaction ($\Delta G_{act} = 0$), it follows that factors influencing the kinetics are mainly the same as those affecting the depletion of interstitial Cu at the precipitate surface, including the built-in voltage (drift) and diffusion. Comparing the kinetics of ALID and RT-LID, diffusivity of interstitial Cu in the low-res Cz sample is 1.5×10^{-6} cm^2 s^{-1} at 120 °C, whereas it is only 4.1×10^{-8} cm^2 s^{-1} at RT. On the other hand, built-in voltages according to the Schottky model are similar at these two temperatures under illumination. Consequently, the faster NR of ALID compared to RT-LID is directly attributable to the increased diffusivity. This result confirms the hypothesis of Ref. 6, where the increased degradation rate of Cu-related ALID was tentatively attributed to the high diffusivity at 120 °C. In addition, correlation between the temperature-dependent diffusivity and NR on one hand and precipitate growth rate on the other hand explain why Cu-LID defect activation was observed to be diffusion-limited in Ref. 5 (where the activation energy is extracted from the temperature dependence of the degradation rate and was therefore observed to reflect the diffusivity of interstitial Cu).

Similar to ALID, the acceleration of the degradation rate with increasing illumination intensity (see Fig. 3) follows almost entirely out of kinetic considerations, with only a minor energetic contribution from the effect of illumination on the effective solubility [through E_{Fp}, see Eq. (28) in Paper I]. The fact that the illumination intensity did not significantly affect the final lifetime in Fig. 3 supports this interpretation, since a change in energetics is expected to alter the precipitate size and density, and consequently the final τ_{eff}. Regarding the difference between experiments and simulations at different intensities, there is almost two orders of magnitude change in the kinetic growth factor, λ_{kin} (see Fig. 2 in Paper I), when intensity is decreased from 1.8 sun to 0.003 sun. However, this change in λ_{kin} does not result in a sufficient decrease in the simulated degradation rate to fully comply with experiments. Nevertheless, the simulation results shown in Fig. 3 can be seen as qualitative evidence that a change in illumination conditions and consequent effects on precipitate charging can theoretically considerably influence the timescale of precipitation and the associated degradation of τ_{eff}.

D. Precipitate size

As mentioned above, the final density and size of precipitates are expected to have a direct impact on the final degraded τ_{eff}. On the other hand, the precipitate densities of Fig. 8 are directly linked to the final precipitate size through the total density of in-diffused Cu atoms in the sample. Figure 10(a) shows a comparison of experimental and simulated final τ_{eff} in the four different experimental cases described in Figs. 2, 4, and 5 (the same samples as in Fig. 9). Consequently, the trend in the final τ_{eff} is explained by the simulated final size distribution of the precipitates, shown in Fig. 10(b). For the low-res Cz sample with $C_{Cu_i}^{init} = 1 \times 10^{14}$ cm^{-3}, corresponding to the lowest simulated final degraded τ_{eff} of 9.3 μs, the model predicts a dominant precipitate radius of 2–3 nm. On the other hand, with the lower $C_{Cu_i}^{init} = 0.5 \times 10^{14}$ cm^{-3}, associated with a higher simulated final degraded τ_{eff} of 29 μs, the dominant radius is higher, 4–5 nm. Since the precipitate size decreases with increasing $C_{Cu_i}^{init}$, the recombination activity of Cu-LID increases superlinearly with respect to the impurity Cu concentration. In the ALID case, both the simulated final degraded τ_{eff} and the precipitate radius reside in-between the two first mentioned, at 10 μs and 3–4 nm, respectively. Finally, the high final simulated lifetime of 40 μs in the case of the low-res FZ sample can be explained by large precipitates with a dominant radius of 14–16 nm.

Comparing the experimental and simulated τ_{eff} of Fig. 10(a) in general, the qualitative trend between simulation and experiment is in agreement, which is important evidence for the precipitation theory of Cu-LID. The agreement between experimental and simulated injection-dependent final degraded lifetimes in Fig. 7 strengthens this conclusion and the link between the final lifetime and the precipitate size. The deviations between the experimental and modeled final lifetimes are so small that they may, in principle, derive for example from uncertainties in the initial Cu concentration, or ambiguity related to the shape of the precipitates. Nevertheless, the assumption of spherical precipitates seems to reproduce the final lifetimes accurately in all four cases with the estimated total Cu concentration.

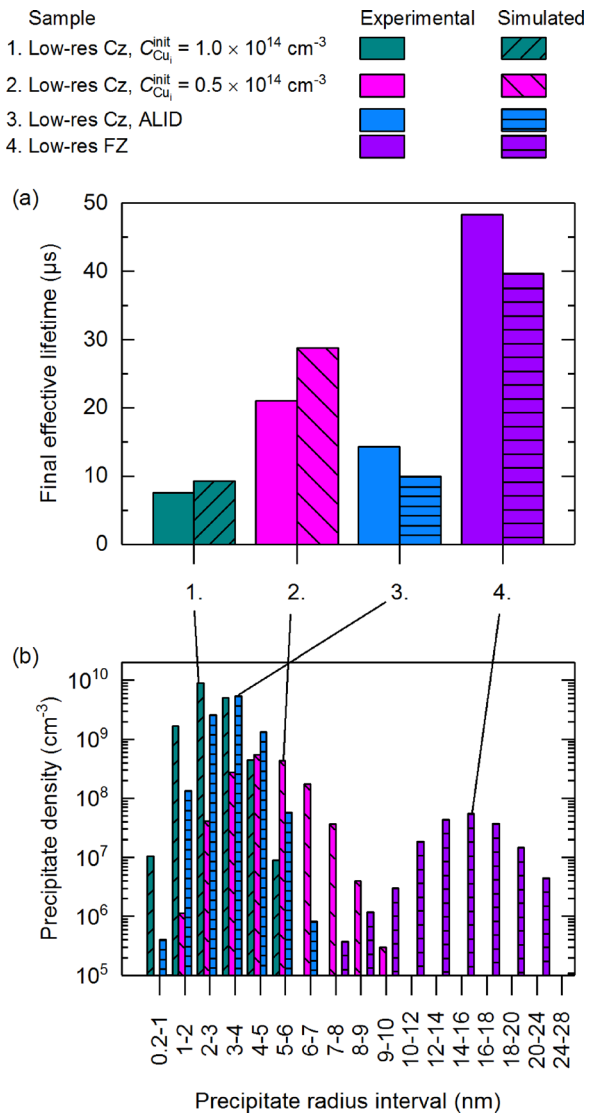

FIG. 10. (a) Experimental and modeled final effective lifetimes, τ_{eff}, of different samples after illumination. Lifetimes are reported at an excess carrier concentration $\Delta n_e = 0.1 \times N_a$. (b) Simulated precipitate radius and density distributions after illumination.

E. Energetic parameters and nucleation mode

As described in Sec. III, the best agreement between simulations and experiments was obtained with energy terms $\Delta G_S = 0$, and $\gamma = 0.615 \times 10^{-4}$ J cm^{-2}. The fitted value of γ is in the same order of magnitude as data of Li,[34] who determined a dependence between γ and Φ_{Bn}. The value obtained interpolating Li's data is $\gamma = 0.76 \times 10^{-4}$ J cm^{-2} for $\Phi_{Bn} = 0.59$ eV, which is in a good agreement considering, for example, uncertainty concerning the exact precipitate shape. Regarding the free energy change per precipitate volume due to strain, ΔG_S, it was found that deviating the value of this quantity from zero always deteriorates the fit. This fact stands in contradiction with the premise of homogeneously nucleating

spherical precipitates, under which the elastic lattice strain would be expected to play a significant role. Possible reasons include either a considerable deviation of the actual precipitate shape from spheres or a sufficient amount of heterogeneous nucleation sites in the studied materials, such as vacancies, dislocations, and/or oxygen precipitate/Si phase boundaries, which minimize the effects of lattice strain. However, with the given total Cu concentration, assuming a strain-minimizing shape such as very thin plates[35–38] would result in a great increase in precipitate radius and/or density. This would cause a substantial increase in the available recombination surface, decreasing the precipitate-limited lifetime up to several orders of magnitude.[4,39] The fact that the spherical shape was shown above to reproduce the experimental results well implies that the shape is closer to spherical than plate-like.

Degradation rate and final lifetime of Cu-LID have been earlier shown to be correlated with density of intentionally grown oxygen precipitates in the bulk.[7] In addition, the spherical precipitate shape has earlier been associated only with heterogeneous nucleation on extended defects that reduce the energetic barrier of nucleation.[35,36] Therefore, the unexpectedly slow degradation of the high-res Cz sample in Fig. 6, and the increase in γ that was necessary to reproduce experiments, can be interpreted to follow from a reduced density of low-energy nucleation sites, such as strained oxygen precipitates,[40] in comparison to low-res Cz. This difference may follow for example from a dissimilar thermal history and/or from the lower O_i concentration (see Table I).[41–43] On the other hand, in low-res FZ reported in Fig. 5, vacancies in the wafer center[44] provide another type of nucleation sites. The same γ in the case of both low-res Cz and low-res FZ implies that the density of heterogeneous nucleation sites does not limit the precipitation process in these materials even though nucleation sites were not intentionally created. Nevertheless, due to simplifications of the model (i.e., spherical precipitate shape and homogeneous nucleation), the energy terms should be considered as effective values. Since final τ_{eff} increased with higher γ, the above conclusion also implies that a part of the negative effects of Cu-LID can be avoided by using Si with a very low density of extended defects.

It should be noted that the assumption that the energy terms remain constant throughout the whole precipitation process might be one source of error in this study. For example, filling of space available on suitable precipitation sites in the Si lattice during precipitate growth could gradually increase the average energy required to include Cu atoms into the precipitates. This effect would lead to a progressive increase in effective solubility [see Eq. (28) in Paper I] during precipitation, which would consequently slow down Cu-LID at longer illumination times. This could be one explanation why the negative slope of Cu-LID curves was shallower in the case of experimental data than simulations (see Fig. 2), and why asymptotic degradation was observed in the experiments at long illumination times.

V. CONCLUSIONS

The comprehensive mathematical model that was proposed for Cu-related light-induced degradation (Cu-LID) in Paper I of the article was compared with experiments in this second part. The fact that the model works directly at the minority carrier lifetime level enabled a straightforward comparison to experimental LID data, against which considerable agreement was found. Both the Cu concentration and doping dependence of Cu-LID can be explained based on the level of supersaturation influencing the nucleation rate and precipitate density. On the other hand, the temperature dependence of Cu-LID follows from the effect of temperature on the diffusivity of interstitial Cu. Although the intensity dependence was reproduced only qualitatively, the simulated degradation rate was very low in the dark due to the dependence of electrostatic repulsion between Cu_3Si precipitates and interstitial Cu on excess carrier concentration. The unexpectedly low nucleation rate in the high resistivity material may be an indication that heterogeneous nucleation sites influence the precipitation process even in Cz and FZ silicon in which these sites have not been intentionally introduced. The simulations revealed a correlation between experimental final degraded lifetime and precipitate size which was found to vary between 2 and 16 nm. This correlation provides a natural theoretical explanation for total recombination activity of Cu-LID increasing superlinearly with increasing interstitial Cu concentration and decreasing with increasing doping concentration and reducing low-energy nucleation site density.

ACKNOWLEDGMENTS

The work has been funded through the European Research Council under the European Union's FP7 Programme ERC Grant Agreement No. 307315. A.I. acknowledges the financial support of Aalto ELEC doctoral school and Alfred Kordelin Foundation. The authors also acknowledge Professor J. Sinkkonen, whose notes are the base for the derivation in Sec. III E of Paper I, and Dr. Chiara Modanese for valuable comments during manuscript writing.

[1]P. S. Plekhanov and T. Y. Tan, Appl. Phys. Lett. **76**, 3777 (2000).
[2]M. D. Negoita and T. Y. Tan, J. Appl. Phys. **94**, 5064 (2003).
[3]W. Kwapil, J. Schön, F. Schindler, W. Warta, and M. C. Schubert, IEEE J. Photovoltaics **4**, 791 (2014).
[4]W. Kwapil, J. Schön, W. Warta, and M. C. Schubert, IEEE J. Photovoltaics **5**, 1285 (2015).
[5]J. Lindroos and H. Savin, J. Appl. Phys. **116**, 234901 (2014).
[6]A. Inglese, J. Lindroos, and H. Savin, Appl. Phys. Lett. **107**, 052101 (2015).
[7]H. Väinölä, E. Saarnilehto, M. Yli-Koski, A. Haarahiltunen, J. Sinkkonen, G. Berenyi, and T. Pavelka, Appl. Phys. Lett. **87**, 032109 (2005).
[8]H. Savin, M. Yli-Koski, and A. Haarahiltunen, Appl. Phys. Lett. **95**, 152111 (2009).
[9]J. Lindroos, Y. Boulfrad, M. Yli-Koski, and H. Savin, J. Appl. Phys. **115**, 154902 (2014).
[10]J. Lindroos, M. Yli-Koski, A. Haarahiltunen, M. C. Schubert, and H. Savin, Phys. Status Solidi RRL **7**, 262 (2013).
[11]T. Heiser, S. McHugo, H. Hieslmair, and E. R. Weber, Appl. Phys. Lett. **70**, 3576 (1997).
[12]A. Richter, S. W. Glunz, F. Werner, J. Schmidt, and A. Cuevas, Phys. Rev. B **86**, 165202 (2012).
[13]J. Schmidt, A. G. Aberle, and R. Hezel, in *Conference Record of the Twenty Sixth IEEE Photovoltaic Specialists Conference - 1997*, Anaheim, California, USA, 29 September–3 October 1997 (Institute of Electrical and Electronics Engineers, New York, 1997), pp. 13–18.
[14]V. V. Voronkov, R. Falster, K. Bothe, B. Lim, and J. Schmidt, J. Appl. Phys. **110**, 063515 (2011).

[15]T. Niewelt, J. Schön, J. Broisch, W. Warta, and M. Schubert, Phys. Status Solidi RRL **9**, 692 (2015).
[16]J. D. Murphy, K. Bothe, R. Krain, V. V. Voronkov, and R. J. Falster, J. Appl. Phys. **111**, 113709 (2012).
[17]K. Bothe, R. Sinton, and J. Schmidt, Prog. Photovoltaics: Res. Appl. **13**, 287 (2005).
[18]J. Schön, T. Niewelt, J. Broisch, W. Warta, and M. C. Schubert, J. Appl. Phys. **118**, 245702 (2015).
[19]D. H. Macdonald, L. J. Geerligs, and A. Azzizi, J. Appl. Phys. **95**, 1021 (2004).
[20]S. Rein, *Lifetime Spectroscopy—A Method of Defect Characterization in Silicon for Photovoltaic Applications* (Springer-Verlag, Berlin, Heidelberg, 2005), pp. 375–377.
[21]F. J. Bottari, W. Montanez-Ortiz, D. C. Wong, P. J. Richter, F. C. Dimock, M. Bowers, and T. Bao, in *2010 35th IEEE Photovoltaic Specialists Conference*, Honolulu, Hawaii, USA, 20 June–25 June (Institute of Electrical and Electronics Engineers, New York, 2010), pp. 001315–001317.
[22]M. B. Shabani, T. Yoshimi, and H. Abe, J. Electrochem. Soc. **143**, 2025 (1996).
[23]H. Väinölä, M. Yli-Koski, A. Haarahiltunen, and J. Sinkkonen, J. Electrochem. Soc. **150**, G790 (2003).
[24]C. Möller, T. Bartel, F. Gibaja, and K. Lauer, J. Appl. Phys. **116**, 024503 (2014).
[25]C. Flink, H. Feick, S. A. McHugo, W. Seifert, H. Hieslmair, T. Heiser, A. A. Istratov, and E. R. Weber, Phys. Rev. Lett. **85**, 4900 (2000).
[26]A. Belayachi, T. Heiser, J. P. Schunck, and A. Kempf, Appl. Phys. A **80**, 201 (2005).
[27]M. O. Aboelfotoh, A. Cros, B. G. Svensson, and K. N. Tu, Phys. Rev. B **41**, 9819 (1990).
[28]P. Hamer, B. Hallam, M. Abbott, and S. Wenham, Phys. Status Solidi RRL **9**, 297 (2015).
[29]N. E. Grant, F. E. Rougieux, D. MacDonald, J. Bullock, and Y. Wan, J. Appl. Phys. **117**, 055711 (2015).
[30]D. Sperber, A. Heilemann, A. Herguth, and G. Hahn, IEEE J. Photovoltaics **7**, 463 (2017).
[31]A. Inglese, J. Lindroos, H. Vahlman, and H. Savin, J. Appl. Phys. **120**, 125703 (2016).
[32]J. Lindroos, Ph.D. thesis, Aalto University, Espoo (2015).
[33]D. Kashchiev, *Nucleation - Basic Theory with Applications* (Butterworth-Heinemann, Oxford, 2000) pp. 17–44.
[34]J. G. Li, Mater. Chem. Phys. **47**, 126 (1997).
[35]M. Seibt, M. Griess, A. A. Istratov, H. Hedemann, A. Sattler, and W. Schröter, Phys. Status Solidi A **166**, 171 (1998).
[36]M. Seibt, H. Hedemann, A. A. Istratov, F. Riedel, A. Sattler, and W. Schröter, Phys. Status Solidi A **171**, 301 (1999).
[37]A. A. Istratov, H. Hedemann, M. Seibt, O. F. Vyvenko, W. Schröter, T. Heiser, C. Flink, H. Hieslmair, and E. R. Weber, J. Electrochem. Soc. **145**, 3889 (1998).
[38]H. W. Guo and S. T. Dunham, Appl. Phys. Lett. **89**, 182106 (2006).
[39]C. Donolato, Semicond. Sci. Technol. **8**, 45 (1993).
[40]R. Falster, V. V. Voronkov, V. Y. Resnik, and M. G. Milvidskii, *High Purity Silicon VIII: Proceedings of the International Symposium*, Honolulu, Hawaii, USA, 3–8 October 2004, edited by C. L. Claeys, M. Watanabe, L. Falster, and P. Stallhofer (The Electrochemical Society, Pennington, NJ, USA, 2004), pp. 188–201.
[41]A. Borghesi, B. Pivac, A. Sassella, and A. Stella, J. Appl. Phys. **77**, 4169 (1995).
[42]H. Takeno, T. Otogawa, and Y. Kitagawara, J. Electrochem. Soc. **144**, 4340 (1997).
[43]J. D. Murphy, M. Al-Amin, K. Bothe, M. Olmo, V. V. Voronkov, and R. J. Falster, J. Appl. Phys. **118**, 215706 (2015).
[44]T. Abe and T. Takahashi, J. Cryst. Growth **334**, 16 (2011).
[45]H. Vahlman, A. Haarahiltunen, W. Kwapil, J. Schön, A. Inglese, and H. Savin, "Modeling of light-induced degradation due to Cu precipitation in p-type silicon. I. General theory of precipitation under carrier injection," J. Appl. Phys. **121**, 195703 (2017).